TU Delft

Bachelor thesis final report

Theoretical model and application of a damped two degree of freedom spring-mass system, moving across a simply supported beam

Anne de Graaf
(4205731)

supervised by
Dr. ir. K.N. van Dalen
ir. A.B. Faragau

June 23, 2018

TU Delft Faculty of Civil Engineering and Geosciences

Summary

In this bachelor thesis a theoretical model is developed for the dynamic loading of a simply supported beam. The dynamic loading is represented by a damped two degree of freedom spring-mass system moving at a constant velocity across the beam (as shown in Figure 1 and 2). The beam is consequently excited by the contact forces and its deflection $w(x,t)$ can be described using the Euler-Bernoulli beam equation. The complete system is described using the following equations of motion:

$$M\frac{\partial^2 u}{\partial t^2} = Mg - Q_1(t) - Q_2(t)$$

$$J\frac{\partial^2 \theta}{\partial t^2} = -\frac{W}{2}Q_1(t) + \frac{W}{2}Q_2(t)$$

$$EI\frac{\partial^4 w}{\partial x^4} + \rho A\frac{\partial^2 w}{\partial t^2} = f(t,x)$$

This set of equations is solved numerically and the numerical model is validated against two limit cases.

Next, two cases of dynamic loading are analysed: first, a passenger train running across a railway bridge, and second, a Hyperloop pod running through a tube at very high speed. By varying the velocity of the respective vehicles, the relation between velocity and beam deflection is illustrated, and between velocity and contact force. However, further analysis is needed to validate these results, and to make sure the results are not influenced by any limitations of the numerical model.

This bachelor thesis shows the complexity of dynamic loading of structures. However simple this model is, the results are quite complex and require careful analysis. Especially the limitations of the numerical model must be taken into account. In future research into the subject, more time should be invested in validating the model and trying to understand and recognize the underlying physical principles of the model in the results.

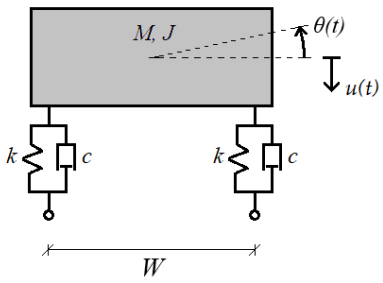

Figure 1: Dynamic system of the vehicle

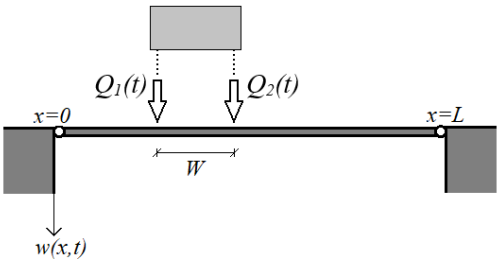

Figure 2: Schematics of the dynamic beam loading

Preface

With this thesis I end a chapter in my life; it marks the end of my Bachelor and my departure from Delft.

I would like to thank my supervisors Andrei Faragau and Karel van Dalen for their time and effort. My meetings with them gave me direction, their knowledge inspired me, and their own enthusiasm sparked mine.

And with that, this thesis also signifies a next chapter; most of the work of this thesis went into mathematics and programming. Two disciplines that, until recently, I didn't realize I liked so much. They are a new-found interest and they will definitely be at the core of my next endeavour.

Contents

Chapter 1

Introduction

The goal of this bachelor thesis is to investigate the effects of dynamic loading on bridge-type constructions using a theoretical model. The loading consists of a simplified vehicle with two degrees of freedom, running over the beam-like bridge construction. The effects are measured only in vertical vibrations of the structure.

The excitation of a bridge can be greatly influenced by the inertia of the vehicle. Taking the full dynamic system of the vehicle into account however, results in a complicated mathematical problem. Previously, a bachelor thesis was done by Bilal Ouchene (Ochene, 2018), investigating dynamic loading by a single mass-spring system. In this thesis this model will be expanded into a damped, two degree of freedom spring-mass system.

The dynamic model of the vehicle is greatly simplified. In general a vehicle, like for example a train, consists of multiple sprung and unsprung masses (the cart, multiple bogies and the (unsprung) wheels). Such a detailed model can be quite complicated to calculate. Given the short time frame of this thesis, the decision was therefore made to use a more simplistic model.

In this thesis a general model will be provided for a vehicle moving across a bridge-type structure. The model will be validated and then applied to two cases: first a train running across a railway bridge. Then, a Hyperloop pod running through an elevated tube-section.

First, an overview of the theoretical model will be provided in Chapter 2. Here the dynamic system of the vehicle will be described and the most important underlying theories and mathematical principles will be laid out. In Chapter 3 the model will be validated and in Chapter 4 the model will be applied to the railway bridge case and the Hyperloop case respectively. The results of Chapter 2-4 will be presented in Chapter 5, followed by Conclusions and Recommendations (Ch. 6).

The Python code of the numerical model is attached in Appendix A. As stated by the Bachelor Thesis requirements, the reports of the intermediate meetings are also appended.

Chapter 2

Theoretical model

2.1 Dynamic system and equations of motion

The vehicle in this model is modelled as a single mass M with inertia J on two wheel axes with wheelbase W (see Figure 2.1). Each wheel axis is modelled as a spring k in parallel with a dashpot c and has a single contact point with the beam. This gives the mass two degrees of freedom: a vertical displacement denoted by $u(t)$ and a rotation around its centre of gravity $\theta(t)$.

The bridge over which the vehicle travels is modelled as a simply supported beam of length L (see Figure 2.2). The vehicle moves at constant velocity v and transfers its load to the beam through two time-dependent forces $Q_1(t)$ and $Q_2(t)$ which are equal to the reaction forces in the wheel axes. As a result of the dynamic loading, the excitation of the beam over x and t is denoted by $w(x,t)$. This yields the following set of equations of motion for the vehicle:

$$M\frac{\partial^2 u}{\partial t^2} = Mg - Q_1(t) - Q_2(t) \tag{2.1}$$

$$J\frac{\partial^2 \theta}{\partial t^2} = -\frac{W}{2}Q_1(t) + \frac{W}{2}Q_2(t) \tag{2.2}$$

Where:

$$Q_1(t) = k\left[u(t) + \frac{W}{2}\theta - w(vt - W, t)\right] + c\left[\frac{\partial u}{\partial t}(t) + \frac{W}{2}\frac{\partial \theta}{\partial t} - \frac{\partial w}{\partial t}(vt - W, t)\right] \tag{2.3}$$

$$Q_2(t) = k\left[u(t) - \frac{W}{2}\theta - w(vt, t)\right] + c\left[\frac{\partial u}{\partial t}(t) - \frac{W}{2}\frac{\partial \theta}{\partial t} - \frac{\partial w}{\partial t}(vt, t)\right] \tag{2.4}$$

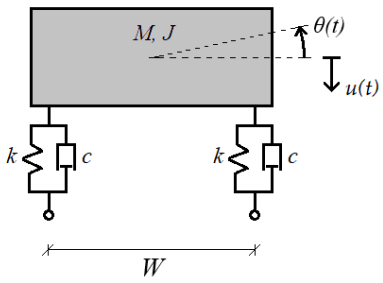

Figure 2.1: Dynamic system of the vehicle

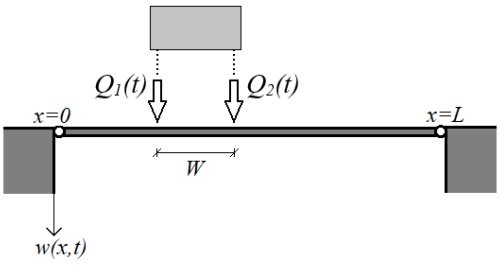

Figure 2.2: Schematics of the dynamic beam loading

The vehicle is assumed to be at rest at $t = 0$. Due to the gravity acting on the mass, there will however be an initial displacement $u(t) = Mg$. This leads to the following initial conditions for the vehicle:

$$u(0) = \frac{Mg}{2k} \qquad \frac{\partial u}{\partial t}(0) = 0 \tag{2.5}$$

$$\theta(0) = 0 \qquad \frac{\partial \theta}{\partial t}(0) = 0 \tag{2.6}$$

2.2 The Euler-Bernoulli beam equation

The dynamic behaviour of the beam is described by the Euler-Bernoulli beam theory (Wikipedia Contributors, 2018).

$$EI\frac{\partial^4 w}{\partial x^4} + \rho A\frac{\partial^2 w}{\partial t^2} = f(t,x) \tag{2.7}$$

Where EI represents the bending stiffness of the beam and ρA the mass per unit length. The forcing $f(x,t)$ is represented by the two wheel loads $Q_1(t)$ and $Q_2(t)$. These loads move with constant velocity v across the beam, which can be expressed by multiplying each load with a Dirac delta function. The location of load $Q_2(t)$ is equal to vt yielding $\delta(x - vt)$. For $Q_1(t)$ this expression is similar but its location is translated to the left by wheelbase W, giving $\delta(x - v(t - W/v))$.

Furthermore, the loading only occurs while the vehicle is on top of the beam. This can be expressed by the Heaviside function H. Load $Q_2(t)$ will be on the beam from $t = 0$ till $t = L/v$. Load $Q_1(t)$, again being translated by W, will be on the beam from $t = W/v$ till $t = (W + L)/v$. This gives the following expression for the forcing $f(x,t)$:

$$f(x,t) = Q_1(t)g_1(x,t) + Q_2(t)g_2(x,t) \tag{2.8}$$

With:

$$g_1(x,t) = \delta\Big(x - v\Big(t - \frac{W}{v}\Big)\Big)\left[H\Big(t - \frac{W}{v}\Big) - H\Big(t - \frac{W+L}{v}\Big)\right]$$

$$g_2(x,t) = \delta\Big(x - vt\Big)\left[H(t) - H\Big(t - \frac{L}{v}\Big)\right]$$

The beam will initially be at rest. This gives the following initial conditions for the beam:

$$w(x,0) = 0 \qquad \frac{\partial w}{\partial t}(x,0) = 0 \tag{2.9}$$

The bending moment in both ends of the beam will be zero. This yields the following boundary conditions for the beam:

$$w(0,t) = 0 \qquad \frac{\partial^2 w}{\partial x^2}(0,t) = 0 \tag{2.10}$$

$$w(L,t) = 0 \qquad \frac{\partial^2 w}{\partial x^2}(L,t) = 0 \tag{2.11}$$

2.3 Solution to the EB beam equation

It is assumed that the deflection $w(x,t)$ of the beam takes the following form, where K denotes the number of modes of vibration of the beam taken into account:

$$w(x,t) = \sum_{k=1}^{K} \varphi_k(x)q_k(t) \tag{2.12}$$

The x-dependency $\varphi_k(x)$ will be the same for any load case, since the variety in deflection modes of the beam are physically determined by the beam's characteristics. This means that the $\varphi_k(x)$ term can easily be determined by solving the homogeneous solution to the EB beam equation (2.7):

$$EI\frac{\partial^4 w}{\partial x^4} + \rho A\frac{\partial^2 w}{\partial t^2} = 0 \tag{2.13}$$

Solving the equation the following expression is found for $\varphi_k(x)$:

$$\varphi_k(x) = C_1 \sin\left(\frac{k\pi x}{L}\right) \tag{2.14}$$

With C_1 a free constant. This expression can then be used to solve the inhomogeneous equation (2.7). By substituting $w(x,t)$ from eq. (2.12) into eq. (2.7) the following equation is obtained:

$$\sum_{k=1}^{K} \varphi_k(x)\frac{\partial^2 q_k}{\partial t^2}(t) + \omega_k^2\varphi_k(x)q_k(t) = \frac{1}{\rho A}f(x,t) \tag{2.15}$$

With eigenfrequency:

$$\omega_k = \sqrt{\frac{EI}{\rho A}}\left(\frac{k\pi}{L}\right)^2$$

.

From the orthogonality principle it follows that:

$$\int \varphi_k(x)\varphi_n(x)dx = \int \sin\left(\frac{k\pi x}{L}\right)\sin\left(\frac{n\pi x}{L}\right)dx = \begin{cases} \frac{L}{2}, \text{ for } k = n \\ 0, \text{ for } k \neq n \end{cases} \tag{2.16}$$

By applying $\int_0^L \dots\ \varphi_n(x)dx$ to both sides of the equation (2.15) the equation reduces to:

$$\sum_{n=1}^{N} \frac{\partial^2 q_n}{\partial t^2}(t) + \omega_n^2 q_n(t) = \sum_{k=1}^{K}\sum_{n=1}^{N} \frac{2}{\rho AL}\Big(Q_1(t)h_1(t)\varphi_n(vt - W) + Q_2(t)h_2(t)\varphi_n(vt)\Big) \tag{2.17}$$

With:

$$h_1(t) = H\Big(t - \frac{W}{v}\Big) - H\Big(t - \frac{W+L}{v}\Big)$$

$$h_2(t) = H(t) - H\Big(t - \frac{L}{v}\Big)$$

Solving the differential equation and considering the trivial initial conditions of the beam, the following expression for q_n is obtained:

$$q_n(t) = \frac{2}{\rho AL}\frac{1}{\omega_n}\int_0^t \sin\left(\omega_n(t-\tau)\right)\Big(Q_1(\tau)h_1(\tau)\varphi_n(v\tau - W) + Q_2(\tau)h_2(\tau)\varphi_n(v\tau)\Big)d\tau \tag{2.18}$$

Using eq. (2.12) and (2.14) this gives the following expression for $w(x,t)$:

$$\begin{aligned} w(x,t) = \sum_{n=1}^{N} \sin\left(\frac{n\pi x}{L}\right)\frac{2}{\rho AL}\frac{1}{\omega_m}\int_0^t \sin\left(\omega_n(t-\tau)\right) \\ \times\Big(Q_1(\tau)h_1(\tau)\varphi_n(v\tau - W) + Q_2(\tau)h_2(\tau)\varphi_n(v\tau)\Big)d\tau \end{aligned} \tag{2.19}$$

Also, solving (2.1) and (2.2) and considering the initial conditions from (2.5) and (2.6):

$$u(t) = \frac{Mg}{2k} + \frac{gt^2}{2} - \frac{1}{M}\int_0^t (t-\tau)\left(Q_1(\tau) + Q_2(\tau)\right)d\tau \tag{2.20}$$

$$\theta(t) = \frac{W}{2J}\int_0^t (t-\tau)\left(Q_2(\tau) - Q_1(\tau)\right)d\tau \tag{2.21}$$

2.4 Numerical solution to the dynamic forcing

Next, the dynamic forcing $Q_1(t)$ and $Q_2(t)$ can be numerically computed by substituting the expression for $w(x,t)$, $u(t)$ and $\theta(t)$ from eq. (2.19) - (2.21) into eq. (2.3) and (2.4). The obtained set of equations are implicit, with $Q_1(t)$ and $Q_2(t)$ appearing on both sides of the equation. This is solved iteratively by using $Q_1(t)$ and $Q_2(t)$ at timestep i to determine $Q_1(t)$ and $Q_2(t)$ at timestep $i+1$:

$$w_i, u_i, \theta_i = f(Q_{1i}, Q_{2i})$$
$$Q_{1i+1}, Q_{2i+1} = f(w_i, u_i, \theta_i, w_i', u_i', \theta_i')$$

The numerical algorithm used to solve the set of equations is written in Python and enclosed in Appendix A. The integrals of eq. (2.19) - (2.21) are evaluated using the trapezoidal method from the Numpy package. The method gives satisfactory accurate results in this case, however for very large spring stiffness and damping coefficient, the model may become unstable if the stepsize h is too large.

The time derivatives of $w(x,t)$, $u(t)$ and $\theta(t)$ in eq. (2.3) and (2.4) are calculated using the backward difference method. This method is very convenient as the derivative at timestep i only depends on the current and previous timesteps and is therefore easy to implement in a programming loop. The method gives satisfactory results in combination with the used stepsize in this case.

The validation of the numerical model will be discussed in the next chapter.

Chapter 3

Validation of the numerical model

The validation of the numerical model takes place in two-fold: first, the model is built up gradually, starting with a very simple load-case (a constant stationary force on a beam), comparing this with the known analytical solution and then expanding the model into a slightly more complex case. Second, once the final model is finished, it is tested against a number of limit cases of which the analytical solution is known. The parameters used for the plots in this chapter do not resemble a real-life application, however they are chosen within the realistic range. The parameters are not necessarily the same for each figure.

3.1 Building up in complexity

The final model is built in nine steps, starting with a very simple model then gradually increasing the complexity with each step. The first step is a single stationary point-load on a beam. Next, this point load may start moving at a constant velocity and finally some dynamic characteristics are added like a spring and a viscous damper, though the load still has no inertia. In these cases, if the velocity is reasonably low, the deflection of the beam can be approximated using the equation for deflection by a stationary load. This relation is also shown in Figure 3.1. Here, the actual displacement of the beam under a moving point-load (the grey arrow) is plotted in blue. It can be seen that the line is closely approximated by the grey line, which shows the displacement by a static load at the same location (indicated by the grey arrow). The higher the damping, the more closely together are the two lines.

The model then is further expanded into two moving constant point-loads (a screen shot is added in Figure 3.2). And then into a single mass-spring system and a double mass-spring system. Finally the two mass-spring systems are coupled and the single mass, two degree of freedom model is achieved.

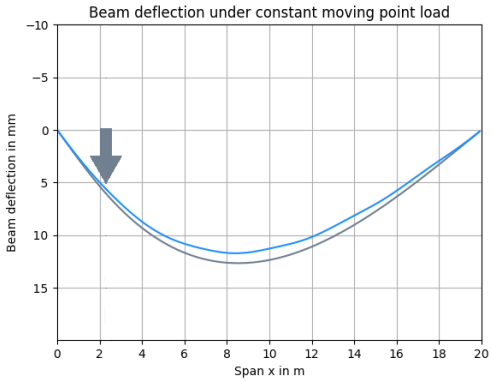

Figure 3.1: Beam deflection under constant moving point load

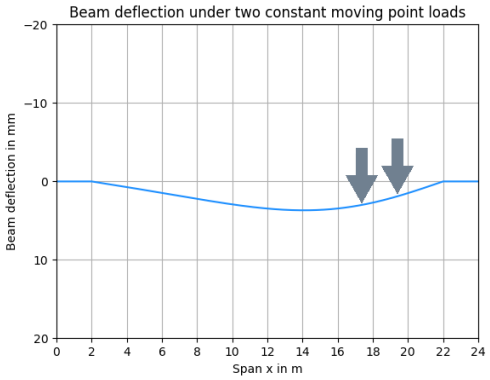

Figure 3.2: Beam deflection under two constant moving point loads

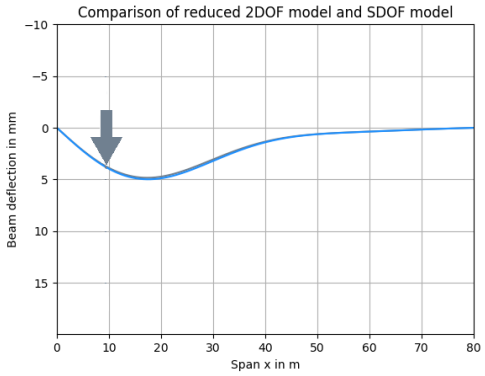

Figure 3.3: Beam deflection under SDOF and 2DOF with wheelbase 1cm

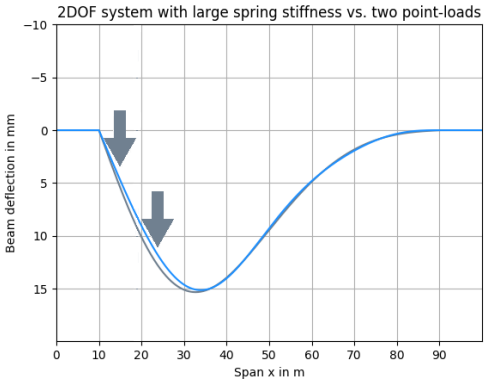

Figure 3.4: Beam deflection under large spring stiffness vs. two moving point loads

3.2 Testing against limit cases

The model will next be tested against two limit cases. First of all, when making the wheelbase very small, the model will effectively reduce to a single mass-spring system. This gives the opportunity to test the two degree of freedom (2DOF) system against the single degree of freedom system (SDOF). Because the 2DOF system has two springs and two dampers, the system is approximately equivalent to a SDOF with double the spring stiffness and damping coefficient. In Figure 3.3 a snapshot of the deflection under a 2DOF system (in blue) and an equivalent SDOF system (in grey) are shown in the same plot. The wheelbase of the 2DOF system is set to 1 cm. The grey plot barely shows, being almost precisely the same as the blue plot. So it can indeed be concluded that the systems are equivalent and the limit case is correct.

The next limit case occurs when the spring stiffness is very large. In this case the model effectively turns into two constant point-loads of $0.5 * mass * g$ each. In Figure 3.4 a snapshot is shown of the dynamic loading of a very stiff 2DOF system (blue) versus loading by two moving point-loads (grey). It can be seen that, however close, the two lines in this case don't completely coincide. This is probably to blame on the fact that not enough modes of excitation were used to calculate the deflection.

3.3 Limitations of the model

In working out the above cases, it really shows the numerical model has its limitations. The biggest of which is that the model becomes unstable for large spring stiffness and/or large damping coefficient. This is caused by the chosen method of numerical integration (trapezoidal method). The integral is determined using discrete time steps and if these time steps are too large, the integral can become very big, making the system unstable. This is obviously limiting for the use of the model as a tool for theoretical analysis.

Another limitation that should be taken into account when using this model, is that the true deflection of the beam is only *approached* using a finite summation of sinuses (modes). It is therefore important to make sure a sufficient amount of modes is taken into account. For instance, the shear forces in the structure can be determined by taking the third derivative of the deflection. In the case considered in this thesis, the structure is loaded by (time-dependent) point loads, which cause abrupt jumps in the shear force distribution. However, if the number of excitation modes are not sufficient, it will not be possible to describe this behaviour, which might lead to misjudging the stresses in the structure.

Chapter 4

Two applications of dynamic loading: passenger train and Hyperloop pod

In this chapter the model will be applied to two real-life cases. The first is a passenger train running across a very long bridge, the second is a Hyperloop pod running through a tube section. The two cases are interesting to compare, as in the first case the vehicle is very heavy and moving at a moderately high speed, whereas in the second, the vehicle is very light, but moving at extremely high speed.

4.1 Passenger train: dynamic loading of a railway bridge

The passenger train model is based on a passenger train with the same characteristics as described by Wang and Markine (2018). The dynamic properties of the train are somewhat simplified as the theoretical model used in this thesis doesn't take secondary suspension into account. The train moves at relatively high speed (200 km/h) so it might qualify to drive on the high speed rail network (HSL). Therefore the HSL Hollandsch Diep bridge is chosen as structure. This bridge has a very large span (105 m) which might give some interesting results. A cross section of the bridge is based on drawings from "Brug Hollandsch Diep HSL-Zuid" (2016) and shown in Figure 4.1. The parameters for the train and bridge are given in Table 4.1. For the calculation of the cross section area and inertia the Cross Section Analyser tool of Hans Welleman is used (Welleman, (2018)).

In Figure 4.3 the deflection of the middle of the bridge is given. From 0.00 till 2.12 seconds the train exerts a forcing on the bridge (see Figure 4.4). After this time the contact forces of the train die out and the deflection of the bridge only consists of free vibrations.

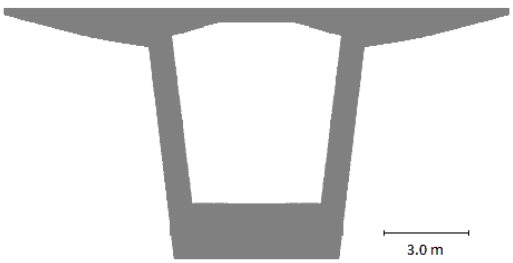

Figure 4.1: Cross section of the Hollandsch Diep bridge

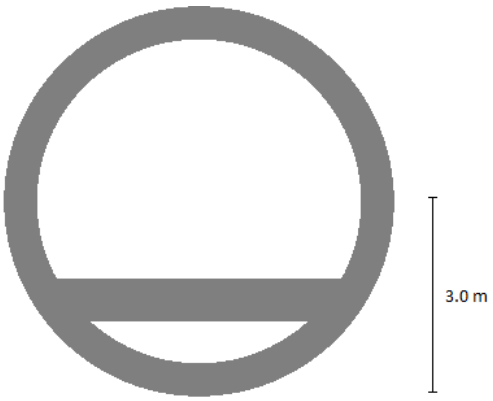

Figure 4.2: Cross section of concrete hyperloop tube

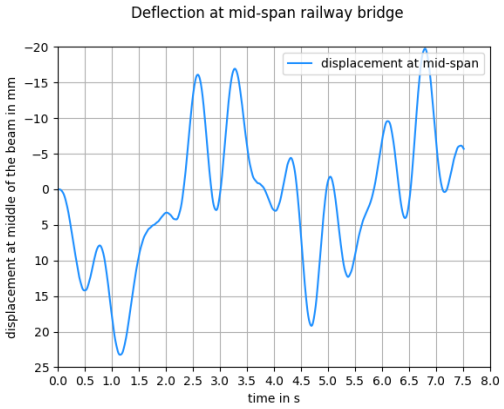

Figure 4.3: Railway bridge deflection at mid-span.

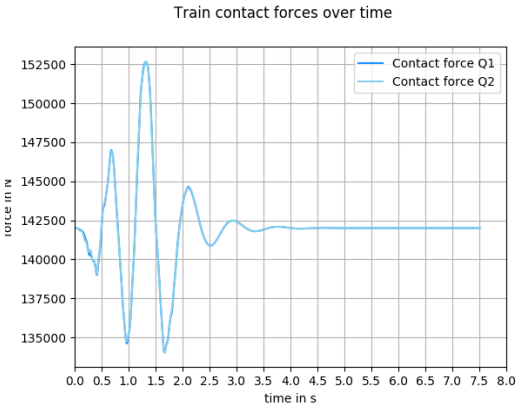

Figure 4.4: Train contact forces over time

4.2 Hyperloop pod: dynamic loading of a concrete tube

The Hyperloop pod model and tube is based on the designs of the Delft Hyperloop 2018 Team, which they kindly shared for the purpose of this Bachelor thesis (The Delft Hyperloop Team, (2018)). These designs did not include the dynamic properties of the pod, so these were estimated on the basis of the Final Design Package of the Delft Hyperloop Team of 2016 (The Delft Hyperloop Team, (2016)). A simplification of the cross section of the tube is shown in Figure 4.2 and an overview of the parameters is given in Table 4.2. Again, the Cross Section Analyser tool was used to calculate the area and inertia of the cross section (Welleman, (2018)).

In Figure 4.5 the deflection of the tube is given at mid-span and the accompanying contact forces are given in Figure 4.6. In this case the period of the vibrations is a lot smaller than for the train case. Because of the high velocity of the Hyperloop, the forced vibrations only take place over a very short period of time. A detail of this period of time is included in Figure 4.7 and 4.8.

Train parameters		
mass	28950.0	kg
inertia	60312.5	$kg.m^2$
velocity	55.6	m/s
wheelbase	12.6	m
spring stiffness	$8.8 * 10^5$	N/m
damping coefficient	$6.0 * 10^4$	$N.s/m$
Bridge parameters		
span	105.0	m
cross sectional area	26.15	m^2
EI	$6.28 * 10^{12}$	$N.m^2$
density	2400.0	kg/m^3

Table 4.1: Parameters for passenger train

Pod parameters		
mass (incl. payload)	8000.0	kg
inertia	2890.0	$kg.m^2$
velocity	277.8	m/s
wheelbase	16.0	m
spring stiffness	$6.0 * 10^4$	N/m
damping coefficient	$4.1 * 10^3$	$N.s/m$
Tube parameters		
span	40.0	m
cross sectional area	11.38	m^2
EI	$1.18 * 10^{12}$	$N.m^2$
density	2400.0	kg/m^3

Table 4.2: Parameters for hyperloop pod

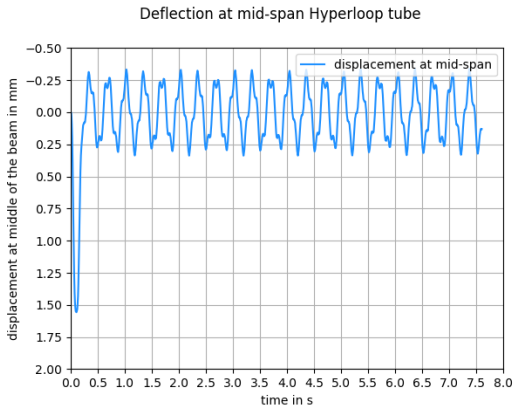

Figure 4.5: Tube deflection at mid-span

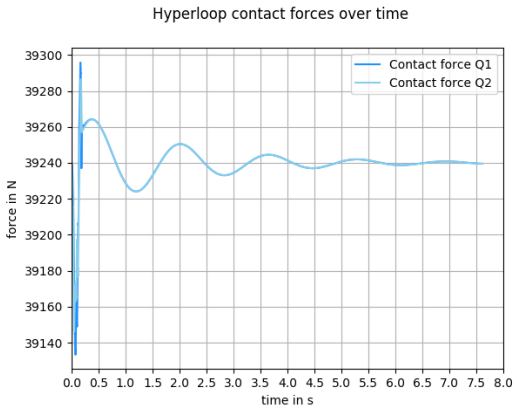

Figure 4.6: Hyperloop contact forces over time

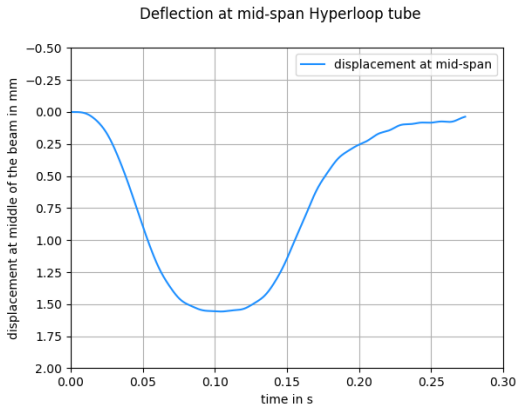

Figure 4.7: Forced vibrations of tube at mid-span

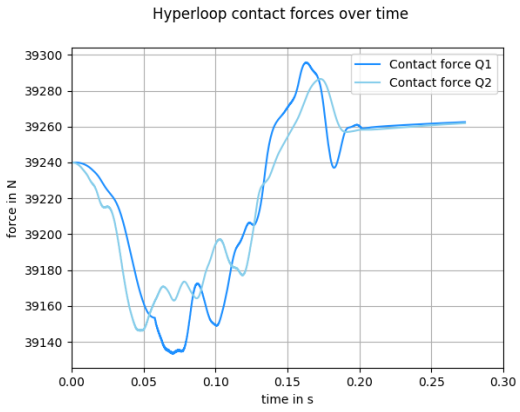

Figure 4.8: Contact forces during forced vibrations

Chapter 5

Results

In order to get a better understanding of the relation between vehicle velocity, beam deflection, and the magnitude of contact forces, a further analysis was done on the two load-cases presented in the previous chapter.

5.1 Influence of velocity on beam deflection

In order to get a better understanding of the effects of the vehicle velocity on the structure, two plots were made showing the extreme structure displacement versus velocity (see Figure 5.1 and 5.2). Knowing the extreme displacements is interesting because it can be an indicator of at what speed the maximum stresses occur in the structure.

Both graphs show a number of peaks, which are plausibly resonance peaks. There seems to be a pattern to these peaks, where they occur at exponentially incremental intervals. In the expression for the eigenfrequency of a mode in eq. (2.15), it can be seen that the eigenfrequency of a mode ω_k is proportional to the square of the mode k^2. This means that the peaks in the graph likely indicate the velocities at which the dynamic contact forces resonate with the various eigenfrequencies of the structure.

Another thing to notice is that the deflection peak(s) at low velocities are slightly higher than the peaks after. At first it was suspected that this might be due to some numerical error. However, reducing the step size did not make a difference, and when reviewing the full animation of the beam excitation at these load velocities, no unnatural behaviour was observed. Further analysis is needed to give a conclusive explanation.

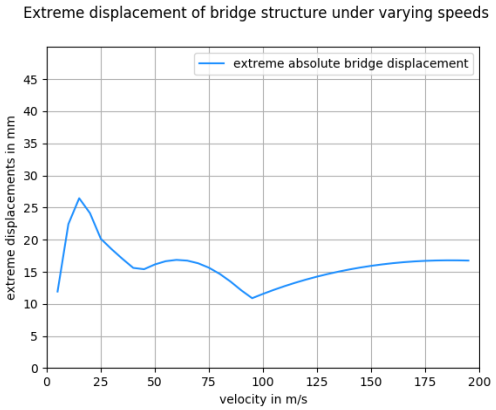

Figure 5.1: Extreme bridge deflection at varying passenger train speeds (5 modes of excitation)

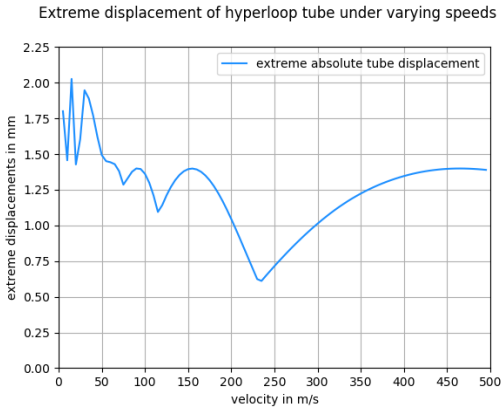

Figure 5.2: Extreme tube deflection at varying Hyperloop pod speeds (5 modes of excitation)

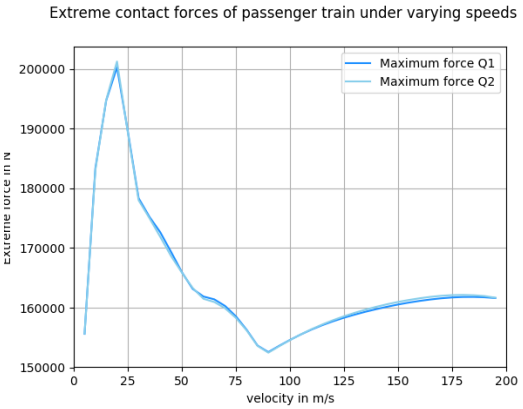

Figure 5.3: Extreme reaction forces at varying passenger train speeds (5 modes of excitation)

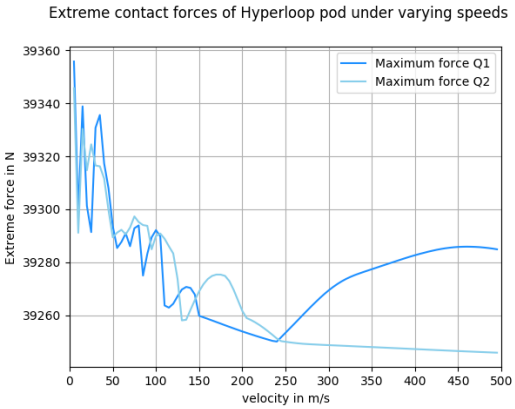

Figure 5.4: Extreme reaction forces at varying Hyperloop pod speeds (5 modes of excitation)

5.2 Influence of velocity on reaction forces

Also the reaction forces from the vehicle are an important load factor for the structure. In Figure 5.3 and 5.4 the maximum occurring contact forces are plotted versus the velocity. It can be seen that the location of peaks and valleys are the same in the forcing graphs as in the displacement graphs. This is logical, as in general a higher contact force will result in a higher displacement.

Chapter 6

Conclusions and recommendations

The behaviour of a structure under dynamic loading is highly complex. The model used in this thesis was simplified to a very large extent. For instance, a real train has primary and secondary suspension and both the bogie and the cart have inertia. Also, the wheels of the train are unsprung and the train has many more degrees of freedom than the two considered here.

But even though the model is largely simplified, that doesn't mean its solution is simple and straightforward; On the one hand the complex nature of the model asks for a proper validation of the solution. On the other hand difficulties can arise because of numerical errors; The two load-cases considered in this thesis were very different: the first case was a heavy, slower moving vehicle, and the second was a light, fast moving vehicle. These extreme parameters of the load-cases caused instability in the numerical program.

It is recommended that when this thesis' subject is further researched, more emphasis is put in analysing the results and getting a good understanding of the model. In this thesis too little time was put in the analysis even though it is in fact perhaps the most interesting part.

Secondly, this model could be used to investigate a number of very interesting things. For instance, instead of just looking at beam deflection and reaction forces, the model could also be used to look into the stresses in the structure. Or, the model could be tested against real measurements of bridge deflection under dynamic loading.

Lastly, the numerical integration method (trapezoidal) used in this thesis leaves some room for improvement. When the model is used to describe heavy vehicles like trains, the model becomes unstable very fast. A more stable numerical method is recommended.

References

Brug Hollandsch Diep HSL-Zuid. (2016, 17 februari). Retrieved May 18 2018, from https://studiosk.nl/projecten/brug-hollandsch-diep-hsl-zuid/

Ouchene, B. (2018). *Dynamische interactie tussen een bewegende massa-veer systeem en een buigligger*. Retrieved from https://repository.tudelft.nl/

The Delft Hyperloop Team. (2016). *Final Design Package*. Courtesy of the Delft Hyperloop Team 2016.

The Delft Hyperloop Team. (2018). *Parameter Sheet*. Courtesy of the Delft Hyperloop Team 2016.

Wang, H., & Markine, V. (2018). Modelling of the long-term behaviour of transition zones: Prediction of track settlement. *Engineering Structures, 156,* 294-304. doi:https://doi.org/10.1016/j.engstruct.2017.11.038

Welleman, J. W. (2018, februari). Windowsprogramma Bitmap Section Analyser. Retrieved May 18 2018, from http://icozct.tudelft.nl/TUD_CT/CT3109/collegestof/inhomogene_doorsneden/

Wikipedia Contributors. (2018, 5 juni). Euler–Bernoulli beam theory. Retrieved May 18 2018, from https://en.wikipedia.org/wiki/Euler%E2%80%93Bernoulli_beam_theory

Appendix A: Numerical model

```
import numpy as np
import math
import matplotlib.pyplot as plt
import matplotlib.animation as animation


## FULL MODEL: 1 MASS 2DOF VEHICLE OVER SIMPLY SUPPORTED BEAM

# input vehicle
mass = 140.0              # kg
velocity = 2.0            # m/s
spring = 5000.0           # N/m
damp = 10000.0            # N.s/m
wbase = 2.0               # m
inertia = 167.0           # kg.m^2

# input beam
span = 20.0               # m
area = 0.4                          # m^2
EI = 90666667.0           # N.m^2
density = 2400.0          # kg/m^3
excitationModes = 5

g = 9.81          # gravitational constant

massOffset = 0.5*mass*g/spring + 0.02    # m

trajectory = span + 2*wbase
# includes beam and land abutment on both ends

# time steps
lowestFreq = np.pi**2 / (span**2) * np.sqrt( EI/(density*area) )
dt = 0.01/lowestFreq
time = np.arange(0, (span+wbase)/velocity+dt, dt)
t1 = int((wbase/velocity)/dt)    # Q1 enters the beam (as time index)
t2 = int((span/velocity)/dt)     # Q2 leaves the beam (as time index)

# x steps
dx = 0.1
x = np.arange(0, trajectory+dx, dx)
x1 = int(wbase/dx)               # beginning of beam (as x index)
x2 = int((wbase+span)/dx)        # end of beam (as x index)

# initializing empty arrays for the numerical calculation
```

```
w = np.zeros((len(time), len(x)))       # w(t,x)
wDiff = np.zeros((len(time), len(x)))   # w'(t,x)

u = np.zeros(len(time))                 # u(t)
u[0] = 0.5*mass*g/spring                # initial condition for u(0)
uDiff = np.zeros(len(time))             # u'(t)

theta = np.zeros(len(time))             # theta(t)
theta[0] = 0                            # initial condition for theta(0)
thDiff = np.zeros(len(time))            # theta'(t)

Q1 = np.zeros(len(time))
Q2 = np.zeros(len(time))
Q1[:2] = 0.5*mass*g
Q2[:2] = 0.5*mass*g

xQ1 = np.zeros(len(time))
xQ2 = np.zeros(len(time))

# phi function
def phi_m(m, x, L):
        phi = np.sin(m*np.pi*x / L)
        return(phi)


for t in np.arange(1, len(time)):

        # determine x location (step) of forces at time t
        xQ1[t] = min( x2, int(round((velocity*time[t])/dx)) )
        xQ2[t] = min( len(x)-1, int(round((velocity*time[t])/dx))+x1 )


        # determine intergrals for u(t) and theta(t) (trapezoidal method)
        int_Q1 = np.trapz( (time[t]-time[0:t+1])*Q1[0:t+1], time[0:t+1] )
        int_Q2 = np.trapz( (time[t]-time[0:t+1])*Q2[0:t+1], time[0:t+1] )

        # determine vehicle displacement u(t) and pitch theta(t)
        # and their derivatives (backward Euler method)
        u[t] = 0.5*mass*g/spring + 0.5*g*time[t]**2 - 1/mass*(int_Q1 + int_Q2)
        uDiff[t] = (u[t]-u[t-1])/dt

        theta[t] = 0.5*wbase/inertia*(int_Q2 - int_Q1)
        thDiff[t] = (theta[t]-theta[t-1])/dt


        # determine beam displacement for m modes of excitation
        for m in np.arange(1, excitationModes+1):

                eigenfreq = m**2*np.pi**2 / (span**2)
                        * np.sqrt( EI/(density*area) )

                phi1 = phi_m(m, velocity*time[t]-wbase, span)
                phi2 = phi_m(m, velocity*time[t], span)

                # accounting for heaviside stepfunction for Q1,
                # integral using trapezoidal method
```

```
            if t>=t1:
              duhamel1 = np.sin( eigenfreq*(time[t]-time[t1:t+1]) )
              int_w1 = np.trapz( phi1*Q1[t1:t+1]*duhamel1, time[t1:t+1] )
            else:
              int_w1 = 0

            # accounting for heaviside stepfunction for Q2,
            # integral using trapezoidal method
            if t<t2:
              duhamel2 = np.sin( eigenfreq*(time[t]-time[0:t+1]) )
              int_w2 = np.trapz( phi2*Q2[0:t+1]*duhamel2, time[0:t+1] )
            else:
              duhamel2 = np.sin( eigenfreq*(time[t]-time[0:t2]) )
              int_w2 = np.trapz( phi2*Q2[0:t2]*duhamel2, time[0:t2] )

            # beam deflection at time step t
            phi = phi_m(m, np.arange(0, span, dx),span)
            w[t,x1:x2] += w[t,x1:x2] + phi*(2/(density*area*span*eigenfreq)
            *(int_w1+int_w2))

        # time derivative of beam deflection at step t (backward Euler method)
        wDiff[t] = ( w[t]-w[t-1] )/dt

        # determine the forces for next timestep
        if t<(len(time)-2):
            Q1[t+1] = spring*( u[t] + 0.5*wbase*theta[t] - w[t, xQ1[t]] )
            + damp*( uDiff[t] + 0.5*wbase*thDiff[t] - wDiff[t, xQ1[t]] )

            Q2[t+1] = spring*( u[t] - 0.5*wbase*theta[t] - w[t, xQ2[t]] )
            + damp*( uDiff[t] - 0.5*wbase*thDiff[t] - wDiff[t, xQ2[t]] )
```

Appendix B: Kick-off meeting report

Kick-off meeting report

7 May 2018

Present:
A. de Graaf
Dr. ir. K.N. van Dalen
ir. A.B. Faragau

Kick-off documentation (startnotitie)
Approved (version May 2, 2018).

Alternative mathematical approach to the problem
Karel has another mathematical approach to the problem. He will send it to me. In case I have enough time left and I'm not fed up with the mathematics yet, I can solve the problem using this approach as well.

Comparing results to NEN-EN norm
I've found out that the NEN-EN norm describes a dynamic load as a static load multiplied by a dynamic factor. This means that dynamic effects are described simply by a load. Comparing this to my own results of dynamic loading can be quite tricky, as I'm taking into account multiple modes of vibration. This means that the momentum line and shear force line are not so easy to determine, meaning that the results are not directly comparable to the dynamic forces described in de norm. Hopefully, however, there will be enough time to look at a few specific cases, which I have to work out separately to find the momentum and shear forces.

The dynamic system of a train or hyperloop
I've set up a dynamic system for a train and a hyperloop. Especially the train system is quite complicated. We've agreed that I will first do the calculations for a single mass, 2DOF system. If this is successful, I will expand my model to a more complicated dynamic system, which will be determined once we get there.
Also, I had some doubt whether a hyperloop would give very interesting results, given that it is quite light-weight and thus perhaps causes less vibrations. However, Karel and Andrei do think it will be interesting to look into.
Karel and Andrei told me the mathematical model I will use in my thesis will be able to describe all interesting dynamic effects of a hyperloop, such as doppler shift etc.

Discussing the work I've done so far
I've done some work on the mathematics, which was good so far, but I got stuck from there. Karel provided some handwritten notes on how to move from here.

First supervisor
The first supervisor will be Andrei.

Appendix C: Interim meeting report and interim assessment

Feedback on Ch.1 Introduction
Change the piece about simplification of the model. (as marked on the print-out).

Feedback on Ch.2 Theoretical model
Eq. 2.10 and 2.11: Boundary-conditions must be space-dependent.
Eq. 2.14: Amplitude is missing. It doesn't drop out until eq. 2.15.
Eq. 2.15: The expression for the eigenfrequency is unconventional. Change into:

$$\omega_n = \sqrt{\frac{EI}{\rho A}} \left(\frac{n\pi}{L}\right)^2$$

Eq. 2.16 and 2.17: Don't write out the expression for Q_1 and Q_2 to keep the equations short and understandable.

Feedback on the mathematics
Andrei provided me with tips on how to solve the remaining mathematics.

Interim report assessment

Content

The academic-writing level shown in the report is very good. The content, up to this point, is clearly organized and concise. The governing equations are correct, clearly written and numbered. Moreover, the figures provided help the reader in understanding the meaning of the equations.

Planning

Regarding the initial planning, Anne is somewhat behind schedule. However, understanding the concept and dealing with the mathematics and physics represents the most challenging part of the project. Therefore, spending more time on this part is completely justified. Regarding this first part of the project, Anne showed a thorough understanding of the mathematics, as well as the underlying physics of it.

Recommendations

At this point, the governing equations have been derived. Also, the solution, up to a system of integral equation (which are solved numerically), has been derived. Our recommendation is that Anne starts implementing the derived equations and solve the system using a numerical software (e.g., Matlab). Due to the limited time, we must make sure that the solution is obtained as soon as possible, such that enough time is left for writing the report.

Date

04.06.2018

Candidate

Anne de Graaf

Supervisors

Andrei B. Faragau

Karel N. van Dalen